electronics

MDPI

Article

Laser Image Enhancement Algorithm Based on Improved EnlightenGAN

Youchen Fan [1,†], Yitong Wang [2,†], Kai Feng [2], Yuntian Liu [2], Yawen Jiang [1], Jiaxuan Xie [3], Yufei Niu [3] and Hongyan Wang [1,*]

[1] School of Space Information, Space Engineering University, Beijing 101416, China; love193777@sina.com (Y.F.); 18810975582@163.com (Y.J.)
[2] School of Space Command, Space Engineering University, Beijing 101416, China; wangyitong953@163.com (Y.W.); fzsyk210112@sina.com (K.F.); guhanhaoyue@163.com (Y.L.)
[3] Graduate School, Space Engineering University, Beijing 101416, China; 18543268891@139.com (J.X.); fionanyf@163.com (Y.N.)
* Correspondence: yhgnaw@163.com; Tel.: +1381-008-9037
† These authors contributed equally to this work.

Abstract: In distance-selected imaging, the contrast of laser images is reduced due to long imaging distances, insufficient laser power, and atmospheric turbulence. An enhancement algorithm based on the EnlightenGAN network is proposed to improve the contrast of laser images. Firstly, the laser images are acquired using a distance selection pass system to establish the laser image dataset and expand the dataset, and the traditional algorithm is used to enhance the images and establish the mapping relationship between low-quality images and high-quality images. The global discriminator based on PatchGAN with the improved VGG model is used to regularize the self-feature retention loss and construct the depth link between the global discriminator and the local discriminator to improve the generalization ability of the model; adjust the attention map to the second layer before the CLB convolution module and also add the residual structure in the second layer CLB to improve the robustness of the model; adopt the idea of gray-scale layering with a low drop and high rise to improve the self regularization mechanism to achieve the enhancement of the key region; finally, use the improved EnlightenGAN to fit the relationship between a low-quality image and high-quality image. Finally, EnlightenGAN is used to fit the relationship between low-quality images and high-quality images, extract laser image features, and enhance low-quality images. The experimental results show that the improved algorithm improves PSNR by 12.3% and 0.7% on average, SSIM by 57% and 10.3% on average, and NIQE by 21% and 13% on average compared to other algorithms and the original EnlightenGAN algorithm, respectively. The algorithm improves the signal-to-noise ratio and contrast of laser images with richer image details. It provides a new idea for pre-processing laser images.

Keywords: laser image enhancement; EnlightenGAN; dual discriminator; self-attention mechanism

Citation: Fan, Y.; Wang, Y.; Feng, K.; Liu, Y.; Jiang, Y.; Xie, J.; Niu, Y.; Wang, H. Laser Image Enhancement Algorithm Based on Improved EnlightenGAN. *Electronics* **2023**, *12*, 2081. https://doi.org/10.3390/electronics12092081

Academic Editor: Gwanggil Jeon

Received: 4 April 2023
Revised: 20 April 2023
Accepted: 26 April 2023
Published: 2 May 2023

1. Introduction

The development of laser technology has been changing rapidly in recent years, and new means of active laser imaging are constantly being produced. However, affected by imaging conditions and noise interference, the contrast of the original laser image is low and cannot directly meet practical needs. Image enhancement algorithms can improve the image's overall and local contrast and highlight the image's detailed information. The enhanced images fit the visual features of the human eye better and are easier for machine identification. Image enhancement algorithms have a wide range of applications in military and civilian fields. The new innovative algorithm targets laser images with low brightness, low contrast, and high noise. With the development of deep learning research and the

expansion of its application in various fields, it also has an excellent performance in the field of laser image enhancement.

Existing laser image enhancement algorithms are mainly enhanced from visual and detail features. The histogram, wavelet transform [1], and Retinex theory are three types of improved traditional algorithms. The histogram mainly enhances the algorithm by expanding the grayscale part with more pixels, the wavelet transform uses a method of decomposing sub-bands and layering processing for enhancement, and Retinex mainly relies on scientific experiments and analysis to enhance images. But these three algorithms require many parameters to be determined for improvement, and their impact and generalization abilities are unclear, which can easily lead to problems such as excessive enhancement, loss of important information, and artificial noise. In recent years, deep learning has been widely used in the image field. LL-Net [2] proposed by Lore et al. was the first to use deep learning in image enhancement. They designed a low-light network depth autoencoder to simultaneously enhance and denoise low-light noisy images. Li et al. [3] proposed a convolutional neural network (CNN) image enhancement method. It takes low-illumination images as the network input and the output results are enhanced using the Retinex [4] model. The method solves the problem of distortion caused by over-enhancement in previous methods, but has limitations when enhancing low-quality low-light images.

Since the introduction of generative adversarial networks (GANs) in 2014 [5], it has been widely used for generating high-quality samples using a unique zero-sum game and adversarial training approach. This has strengthened the feature learning and representation abilities of GANs, making it applicable in various fields such as computer vision. However, the lack of paired data for supervised learning makes it difficult to represent the performance. Zhu et al. designed a cyclic consistent adversarial network (Cycle GAN) based on GANs and pairwise learning [6]. It overcomes the shortage of GANs but is prone to the loss of image information and cannot satisfy the structural similarity between the generated image and the real image. In 2021, the EnlightenGAN model was proposed, and it does not require paired training sets. One attention-guided U-Net [7] generator and one global–local discriminator are included, and excellent performance is achieved on a range of standard test data. However, in the encoding–decoding stage, U-Net extracts different levels of features after multiple down-sampling and up-sampling. This can easily distort the generated images [8], especially for darker low-light images, and make it difficult to restore the image detail information. In addition, the generated image tends to have a single color, and unknown artifacts are generated during the enhancement process. The laser image does not guarantee the same effect as other datasets do [9].

To solve the above problems, the paper takes improving the generalization ability of unsupervised deep learning models on laser image datasets as the starting point. It combines the advantages of such models with a newly constructed laser image dataset to study low-light laser image enhancement techniques. The main contributions are as follows:

1. The algorithm is optimized and improved based on the EnlightenGAN model, and its loss function is redesigned to improve the generalization ability and enhancement effect of the model.
2. A deep connection between the global discriminator and the local discriminator is established on the original structure of the EnlightenGAN model, allowing the global loss of the global discriminator to better serve the local optimization of the local discriminator.
3. A new self-regularized attention mechanism applicable to laser images is established. The convolution mode of downsampling is improved to fuse the attention features and the original image features using residuals.

2. Proposed Algorithm

The EnlightenGAN model employs an attention-guided [10] U-Net as a generator and uses a dual discriminator to guide the global and local information and a self-feature

preservation loss to guide the training process, maintaining texture and structure [11], as shown in Figure 1. In this section, we focus on two important building blocks: the global–local discriminator and the self-feature retention loss.

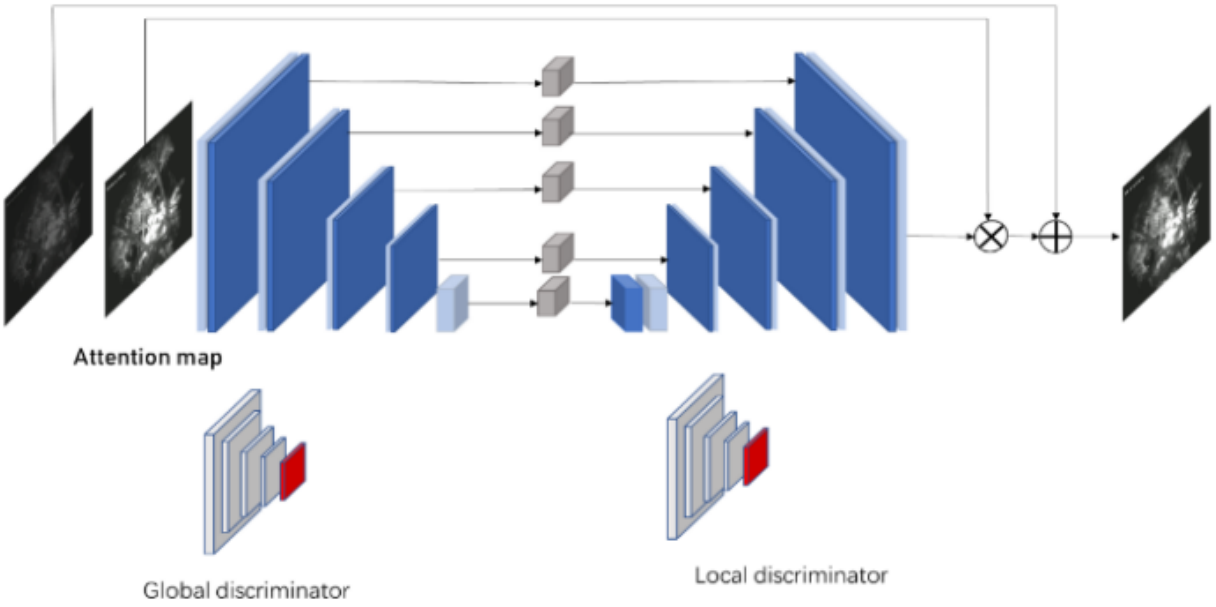

Figure 1. EnlightenGAN model diagram.

2.1. Global–Local Discriminator

In the original GAN, there is a generator that is responsible for generating target samples from Gaussian samples, while there is also a discriminator that is responsible for determining whether the input image is a target sample. The discriminator and the generator have their respective optimization schemes. The discriminator reduces the loss by increasing the correct rate of real samples and decreasing the accuracy of incorrect samples, while the generator reduces the loss by increasing the correct rate of incorrect samples. The optimization function is as follows:

$$\max_{D} V(D,G) = E_{x\sim P_d(x)}[\log(D(x))] + E_{z\sim P_z(x)}[\log(1 - D(G(z)))] \quad (1)$$

$$\min_{G} V(D,G) = E_{z\sim p_z(z)}[\log(1 - D(G(z)))] \quad (2)$$

D represents the discriminator, G represents the generator, and V represents the difference between the real data and the generated data. x is the target distribution image; z is the Gaussian input sample, where E is the expectation; p(x) and p(z), respectively, refer to the distribution of the target sample and the random Gaussian sample. D(x) generates the probability for whether an image is true, G(x) generates a new image, max V represents maximizing the ability of the discriminator to identify the real data or the generated data, and min V represents minimizing the ability of the discriminator to identify the real data or the generated data.

In the input image, the global discriminator often fails to achieve individual enhancement of the local area [12]. Therefore, in order to adaptively enhance local regions and improve the global illumination, we propose a global–local discriminator structure in the model.

The global discriminator uses PatchGAN [13] for true–false discrimination. The authors of the original paper modified the loss function of the standard GAN. The relative meaning is that it considers both the probability that fake data are more real than real data

and the probability that real data are more real than fake data. The function of the relative discriminator is:

$$\begin{cases} D_{Ra}(x_r, x_f) = \sigma(C(x_r) - E_{x_f \sim P_{fake}}\ [C(x_f)]) \\ D_{Ra}(x_f, x_r) = \sigma(C(x_f) - E_{x_r \sim P_{real}}\ [C(x_r)]) \end{cases} \tag{3}$$

In the formula above, C is the discriminator network; x_r and x_f are sampled from the true and false distributions, respectively; σ denotes the sigmoid function [14]; the σ function is replaced by the least squares GAN (LSGAN) loss. In these two formulas, the first is the loss of the discriminator. When a real image is correctly identified and a generated fake image is identified as fake, the discriminator's loss decreases. Conversely, when a real image is incorrectly identified or a generated fake image is identified as real, the loss increases. The second formula is the loss function of the generator. When a real image is misidentified and a generated fake image is identified as real, the generator's loss increases [15]. The final loss functions of the global discriminator D and generator G are as follows:

$$\begin{cases} L_D^{Global} = E_{x_r \sim P_{real}}\ [(D_{Ra}(x_r, x_f) - 1)^2] + E_{x_f \sim P_{fake}}\ [D_{Ra}(x_f, x_r)^2] \\ L_G^{Global} = E_{x_f \sim P_{fake}}\ [(D_{Ra}(x_f, x_r) - 1)^2] + E_{x_r \sim P_{real}}\ [D_{Ra}(x_r, x_f)^2] \end{cases} \tag{4}$$

The local discriminator mainly addresses the need for some local regions to be enhanced differently from other parts. A total of 5 random patches are cropped at a time from the output image and the real image. Then, their truth is distinguished. The difference between this and the global discriminator is that the local discriminator does not use the relative discriminator function, but still uses the original discriminator function [16]. Here, the unmodified LSGAN is used as the adversarial loss:

$$\begin{cases} L_D^{Global} = E_{x_r \sim P_{real-patches}}\ [(D(x_r) - 1)^2] + E_{x_f \sim P_{fake-patches}}\ [(D(x_f))^2] \\ L_G^{Global} = E_{x_f \sim P_{fake-patches}}\ [(D(x_f) - 1)^2] \end{cases} \tag{5}$$

This global–local discriminator structure ensures that all local patches of the enhanced image look like true normal light, which is the key to avoiding local overexposure or underexposure.

2.2. U-Net Generator Guided with Self-regularized Attention

U-Net has achieved great success in semantic segmentation, image recovery, and enhancement. U-Net preserves rich texture information by extracting features from different depth layers at multiple levels, and synthesizes high-quality images using multi-scale contextual information [17].

The adoption of U-Net as a generator backbone network further proposes an easy-to-use network of attention mechanisms for U-Net. In low-light images with spatial variations in light, we prefer to enhance the dark areas rather than the light areas so that the output image is neither overexposed nor underexposed. Therefore, the illumination channel I of the input RGB image is normalized to [0, 1]. Then, 1 to I (the difference between elements) is used as the self-normalized attention map. The attention map is resized to fit each feature map and multiplied with all intermediate feature maps and the output image.

The attention-guided U-Net generator is implemented by 8 convolutional blocks, each consisting of two 3 × 3 convolutional layers, followed by LeakyReLu and batch subsumption layers. In the up-sampling phase, the standard inverse convolution layer is replaced with a bilinear up-sampling layer plus a convolutional layer to reduce the tessellation effect.

3. Model Improvement

3.1. Limitations and Ideas

3.1.1. The Global Discriminator Is Not Related to the Local Discriminator

In the original model, the global discriminator discriminates the entire generated image, and the local discriminator randomly prunes five small fragments from the generated image for discrimination. We contact both the global discriminator and the local discriminator to better train the model for sparsely generated image patches and improve model generalization.

3.1.2. The Self-regularized Attention Is Inconsistent with the Laser Images

In the self-regularized attention mechanism of the original model, more attention is paid to the enhancement of dark regions and the enhancement of bright regions is weakened. Regions with small gray levels will have good enhancement effects, whereas regions with large gray levels will have no obvious enhancement effect. The major differences between the laser dataset and other datasets are that the laser-imaged images do not need to highlight certain dark regions, but the original methods will erroneously highlight those regions.

3.1.3. Refine the Modulus of the Dark Channel

We find that merging the dark channel module in advance can better improve the generalization capability of the model. So, the position of the dark channel module is refined, and on this basis, we also add a residual part to avoid exploding the gradient of the entire model.

3.2. Strong Connection between Global Discriminators and Local Discriminators

Establishing a strong connection between the global and local discriminators further improves the optimization capability of the model. This improved method is proven to be capable of improving the local loss of complex texture images, as shown in Figure 2.

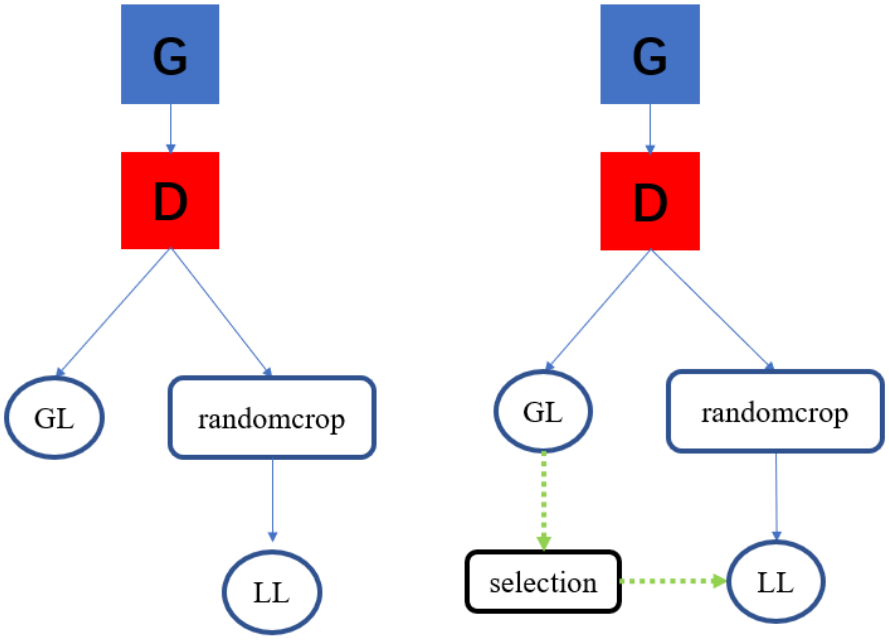

Figure 2. Schematic of the algorithm enhancement.

G represents the generator, D represents the discriminator, GL represents the global loss, randomcrop represents the random cut, LL represents the local loss, and selection represents the selection based on the global loss. The purpose of this paper is to add the strong connection between global and local loss based on the original EnlightenGAN model,

which facilitates the computation of the region with a large global loss when computing the local loss.

Both the global discriminator and the local discriminator are based on the PatchGAN model, and their key feature is that they are replaced with full convolution networks. The discriminator of the joint GAN model maps the input to a real number, i.e., the probability that the input sample is a real sample, and PatchGAN maps the input to an $N \times N$ matrix. In the matrix, value represents the probability of each patch being a real sample, the average of $X_{i,j}$ is the final output of the discriminator, and X is in fact the feature map of the output of the convolution layer. The feature map allows us to track back to a certain position in the original image and observe how much influence that position has on the final output.

This essay establishes the relation between two discriminators on the original base. The global discriminator finds the position with the largest likelihood difference in the patch and extracts the corresponding image position. The corresponding position in the local discriminator is first clipped, and then it is randomly clipped, optimizing local generation. Figure 3 shows that after obtaining the maximum index, the block of images with the largest difference in likelihood is extracted from the original image and then placed in the local discriminator together with the randomly cropped image block.

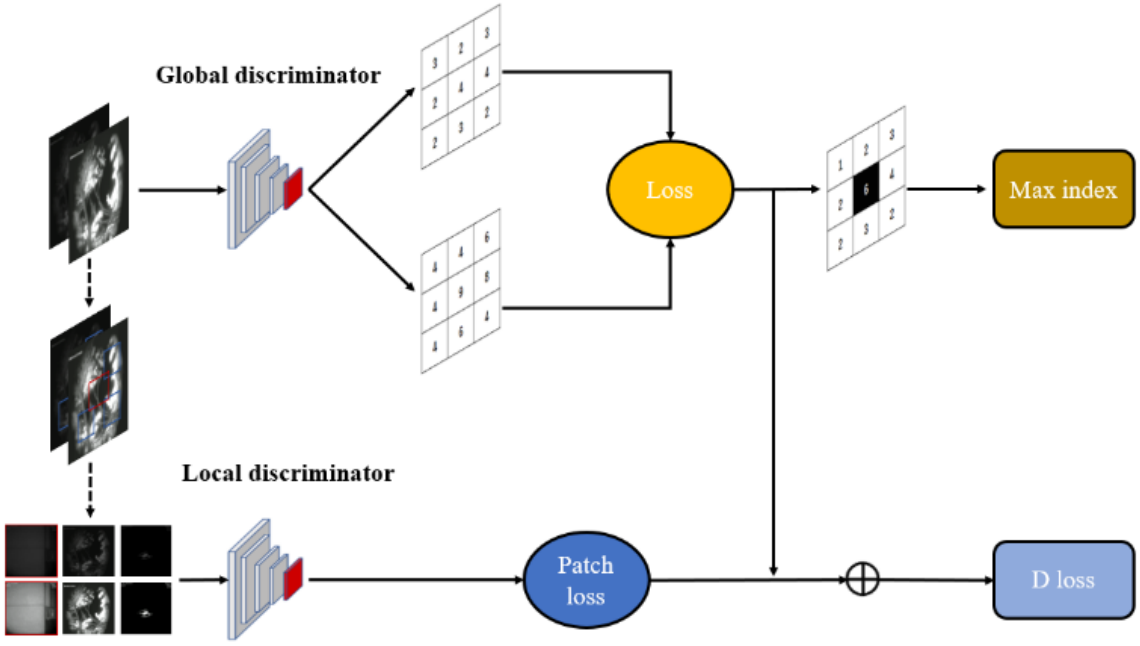

Figure 3. Global–local discriminator.

3.3. Down-sampling Convolution Module Fitting

Downsampling can be commonly understood as shrinking the image and reducing the number of sampling points of the matrix, which serves to reduce the computational effort, reduce information redundancy, and increase the perceptual field. The network implements downsampling by several successive CLB convolutional modules, each consisting of one convolutional kernel, one LeakyReLu activation function in series, and one BN. The features extracted by multilayer convolution have stronger semantic properties compared with other methods.

The original network directly adds attention modules from different scales to the feature map after down-sampling. This attention mechanism has not been extracted by the convolution module, and will lose some of the local detailed textures when merged with the upsampled image. It greatly affects the fusion of features, and so this paper makes targeted improvements for that portion of the locally lost textures.

As shown in Figure 4, the order of the attention map is flexibly adjusted and the attention map is adjusted before the second layer of the CLB convolution module, while

the residual structure is introduced in the second layer of the CLB and the network is made deeper by two constant mappings of the skip connection and activation function. In this way, the attention map can better integrate the original feature map and improve the robustness of the model.

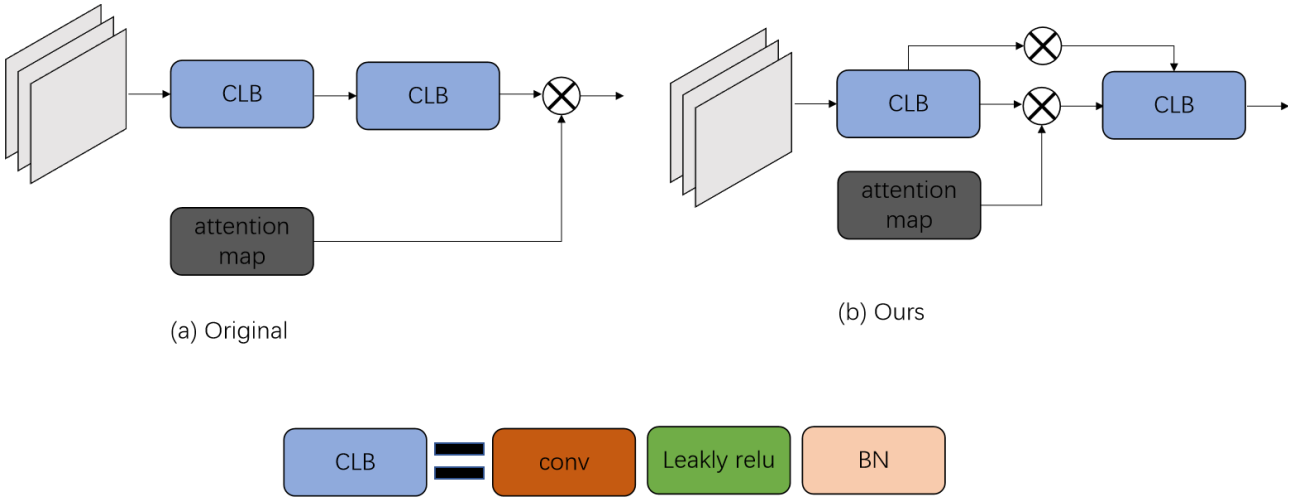

Figure 4. Schematic diagram after fitting the down-sampling convolution module fitting.

3.4. Self-regularized Attention Mechanism

There are a few "dark regions" in the laser data that do not need to be improved. The original model aims to enhance all the low pixels and weaken the high pixels. It does not work directly on our dataset.(Figure 5) shows the effect of applying the model to the original self-regularized attentional diagram. The weights of the dark regions are much larger than those of the non-dark regions, and it does not achieve the expected effect.

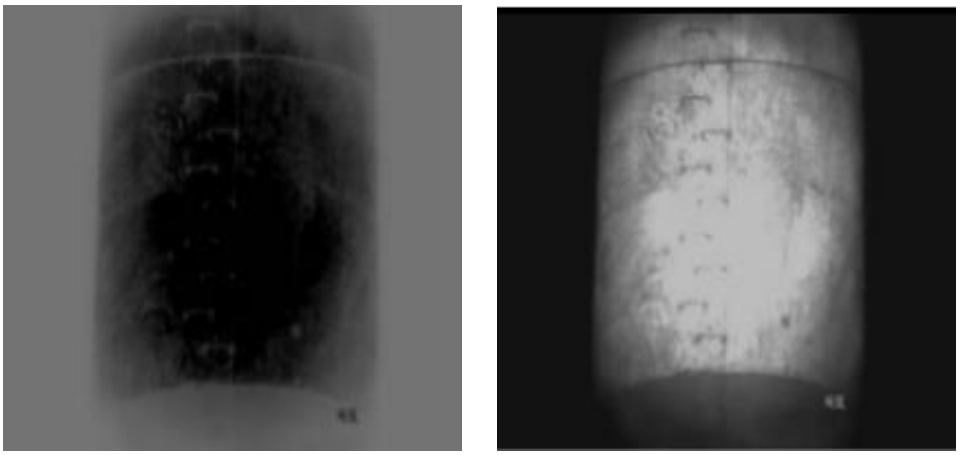

(**a**) (**b**)

Figure 5. Image comparison results. (**a**) Original self-regularization; (**b**) Improved self-regularization.

The original self-regularized attention mechanism is similar to threshold image segmentation in image processing [18]; a novel mechanism is therefore proposed in this paper using this idea.

Consider threshold segmentation to be a function operation:

$$T = T[x, y, p(x, y), f(x, y)] \tag{6}$$

In our method:

$$T = \sigma(f(x, y)/255).f(x, y) \tag{7}$$

The formula is as follows: x and y represent the horizontal and vertical coordinates of the pixel, p(x, y) represents the local features of the pixel, and f(x, y) represents the grey value of the pixel.

After thresholding, the image is defined as follows:

$$g(x,y) = \begin{cases} 0, & f(x,y) < T_1 \\ f(x,y)/255, & T_1 < f(x,y) < T_2 \\ 1 - f(x,y)/255, & f(x,y) > T_2 \end{cases} \quad (8)$$

where $g(x, y)$ denotes the grayscale value of the processed image pixels, and T_1 and T_2 denote the different pixel thresholds. By adopting a new method of autoregulation, i.e., setting a threshold, when it is below the threshold, a low-drop and high-rise attention method is adopted; when it is above the threshold, a low-rise and -fall method is adopted. The improvement in "dark regions" is avoided. Figure 5 shows the comparison between the original self-regularization and the enhanced self-regularization.

4. Experiment and Analysis

4.1. Experiment Design

4.1.1. Experimental Data and Parameter Tuning

The excellent effect of laser-range-gated technology [19] in removing atmospheric backscatter and adjusting system distance has led countries to place great emphasis on relevant research and equipment development. In all countries, the application of range-gated imaging has become the priority imaging method when detecting targets. China, on the other hand, is still at the stage of theoretical research and experimental demonstration. A series of laser datasets is generated over the course of the experiments. For research into the follow-up processing of the laser images obtained, related projects are being carried out by large laboratories.

To assess the performance of this algorithm, unprocessed nighttime laser videos are deconvolved, and 927 high-luminance images and 642 low-luminance images are obtained. All of these images are converted to PNG format and set to 600 × 400 pixels.

Following the training pattern of the original algorithm, we first train 100 iterations with a learning rate of (1×10^{-4}), and then we train 100 iterations with a linear attenuation of zero. The Adam optimizer is used.

4.1.2. Experimental Setting

Table 1 shows the hardware and software setups used in the experiment. The batch size of the EnlightenGAN program is fixed at 32 in this training environment, and the ratio of the training set, the verification set, and the test set is fixed at 6:3:1.

Table 1. Hardware and Software Configurations.

Hardware or Software	Technical Parameters
operating system	Window 10 × 64 Home
GPU	NVIDIA GeForce RTX-3090
CPU	Intel(R) Xeon(R) Silver 4116
memory	32 GB
deep learning libraries	Pytorch
programming language	Python

4.2. Experimentally Measured Indicators

There are three indices used in the experiment to assess the experimental results: NIQE (Natural Image Quality Evaluator) [20], SSIM (Structural Similarity) [21], and PSNR (Peak Signal to Noise Ratio) [22].

4.2.1. NIQE

NIQE, also known as the no-reference image assessment index, is an assessment metric to compensate for all-reference assessment indexes (such as PSNR and SSIM). This primarily uses the regularized NSS model [23] for extracting image features, and these features are taken as input to the MVG model [24]. The distance to the quality perception features extracted from the natural landscape is computed to measure the effect of the image. The lower the NIQE value, the better the quality of the evidence image.

4.2.2. SSIM

SSIM, also called structural similarity, is a metric for measuring the similarity between two input images. This method primarily takes the luminance, contrast, and structural attributes of the objects in the image as the main metrics for measuring similarity. In our experiment, the enhanced image and metadata are used for SSIM evaluation. The greater the similarity, the better the enhancement algorithm.

$$SSIM(x,y) = \frac{(2\mu_x\mu_y + c_1)(2\sigma_y + c_2)}{(\mu_x{}^2 + \mu_y{}^2 + c_1)(\sigma_x{}^2 + \sigma_y{}^2 + c_2)} \tag{9}$$

u_x and u_y represent the mean of images X and Y, respectively; σ_x and σ_y represent the standard deviation of images X and Y, respectively; $\sigma_x{}^2$ and $\sigma_y{}^2$ represent the variance of images X and Y, respectively; C_1 and C_2 are constants.

4.2.3. PSNR

PSNR, also known as the peak signal-to-noise ratio, is an objective standard for assessing image quality. It primarily represents the ratio of the maximum possible signal power and the destructive noise power that affects the accuracy of its representation.

Given a clean image and a noisy image of dimension, where *I(i,j)* and *K(i,j)* are the gray levels of the pixels at position *(i,j)* in the original image, respectively, the mean square error is defined as

$$MSE = \frac{1}{mn}\sum_{i=0}^{m-1}\sum_{j=0}^{n-1}[I(i,j) - K(i,j)]^2 \tag{10}$$

Then, PSNR may refer to:

$$PSNR = 10\log_{10}(\frac{MAX_I^2}{MSE}) = 20\log(\frac{MAX_I}{\sqrt{MSE}}) \tag{11}$$

4.3. Ablation Experiment

According to the feature map redundancy of the Ghost Convolutional layer, it can be inferred that the deep feature map is not suitable for feature redundancy inference using linear calculation. Therefore, the replaced convolutional layers in the experiment are all backbone network convolutional layers close to the input layer. The parameter settings such as the number of Ghost Convolutional layers replaced, training time, and recognition rate in the experiment are shown in Table 2.

The ablation experiment [25] is set-up to test the efficacy of the algorithm. The effects on image enhancement in this group of experiments without thresholded segmentation [26], the fit of the down-sampling module, and the contact with the global and local discriminators are compared, and the experimental results are shown in Figure 6.

Table 2. Comparison of Evaluation Indexes of Ablation Algorithm.

NIQE	Without Threshold	Without Connection	Without Down-Sampling	EnlightenGAN+
tree	13.4	14.5	13.1	12.4
UAV	23.6	25.8	24.8	22.5
wall	13.7	15.6	14.3	12.6
PSNR	Without threshold	Without connection	Without down-sampling	EnlightenGAN+
tree	26.5	23.2	25.9	28.7
UAV	37.3	30.8	38.4	42.8
wall	27.1	26.3	27.3	28.9
SSIM	Without threshold	Without connection	Without down-sampling	EnlightenGAN+
tree	0.43	0.24	0.36	0.44
UAV	0.84	0.57	0.80	0.95
wall	0.43	0.36	0.41	0.48

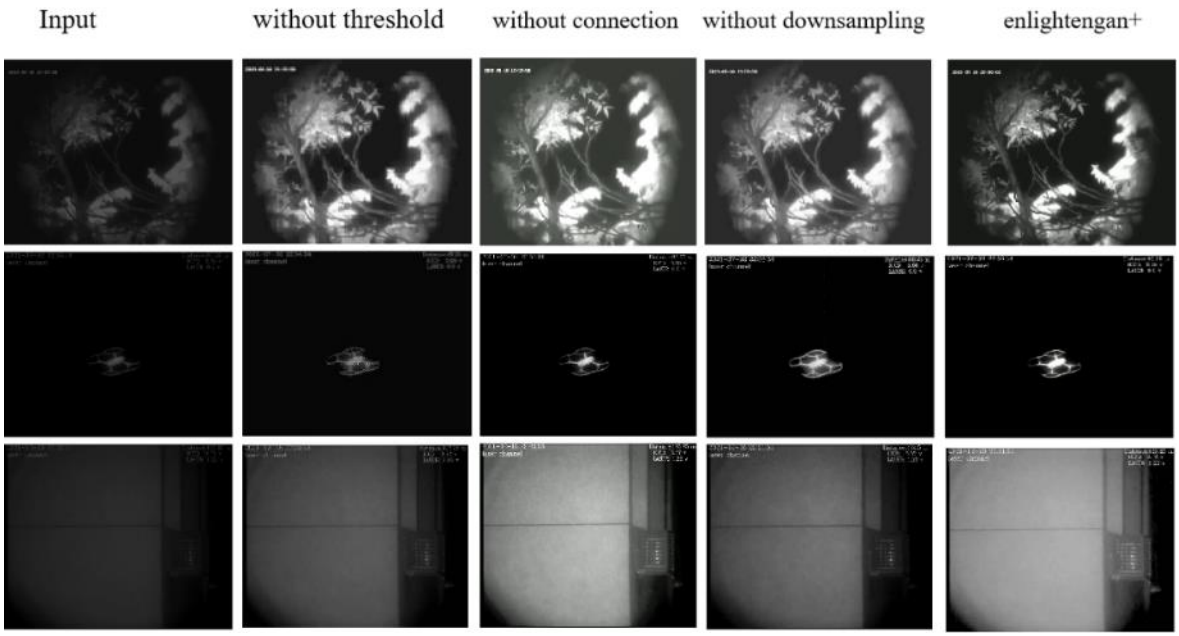

Figure 6. Comparison plot of the results of the ablation experiments.

The NIQE, SSIM, and PSNR of the original method and the improved method are compared to check the efficiency of the algorithm. Table 2 shows the experimental results.

The results of the ablation experiments show that the improved method achieves some results under evaluation indices such as NIQE, PSNR, and SSIM. Self-regularized attention and down-sampling enhancement have similar effects on quantitative indices. But after local connectivity enhancement is removed, it has a larger impact on the model indices. It demonstrates that local connectivity has a larger impact on various indices of the model and can ameliorate model deficiencies very well. Particularly, below the peak signal-to-noise-ratio index, good results are obtained.

4.4. Comparison Experiment

In addition, our experiment compares the contrast effects of different reinforcement algorithms with EnlightenGAN and EnlightenGAN+. To ensure comparability and fairness

of the experiment, when different algorithms are used, they are all performed according to the same training strategy. Figure 7 shows the experimental results.

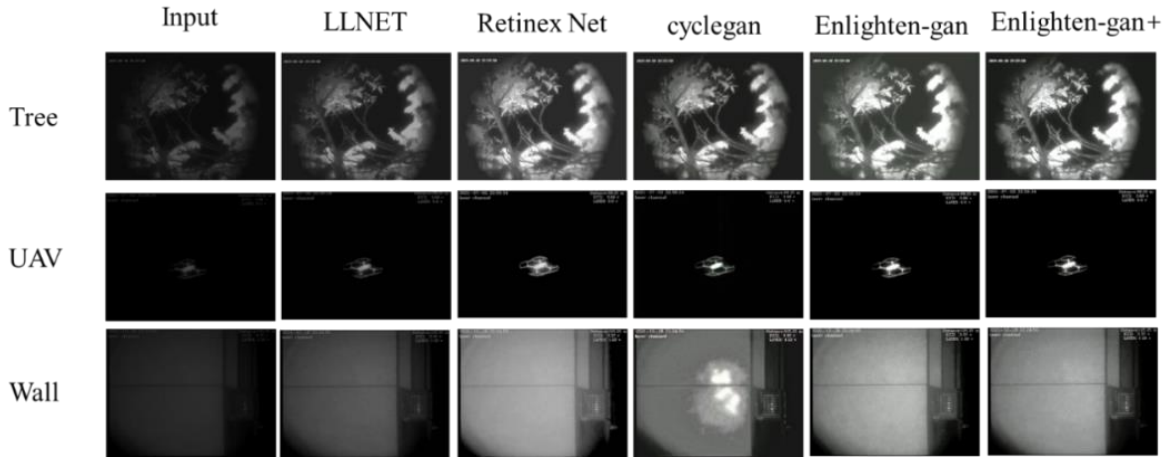

Figure 7. Comparison of different algorithms' effects.

As can be seen in the figure, in comparison to other enhancement algorithms, the algorithm in this paper can produce enhanced images with higher contrast and lower distortion, and achieve a better enhancement effect on nighttime laser image data.

The NIQE, SSIM, and PSNR of different algorithms and the method proposed in this paper are compared to check the efficiency of the algorithm.

The experiment is designed to calculate the NIQE, SSIM, and PSNR of the results obtained by different algorithms and the method proposed in this paper, and to test the efficiency of the algorithms by comparison. Table 3 shows the experimental results.

Table 3. Comparison of Different Algorithms' Measured Indices.

NIQE	CycleGan	LLNET	RetinexNet	EnlightenGAN	EnlightenGAN+
tree	16.8	13.8	12.3	13.7	12.6
UAV	25.1	24.1	23.1	24.4	22.7
wall	13.5	13.9	14.2	13.5	12.4
PSNR	CycleGan	LLNET	RetinexNet	EnlightenGAN	EnlightenGAN+
tree	27.1	26.2	26.9	27.4	27.7
UAV	28.3	31.8	39.4	41.8	42.5
wall	28.1	28.1	27.8	28.9	28.6
SSIM	CycleGan	LLNET	RetinexNet	EnlightenGAN	EnlightenGAN+
tree	0.48	0.66	0.36	0.35	0.46
UAV	0.26	0.29	0.80	0.95	0.96
wall	0.21	0.18	0.41	0.44	0.50

Based on the data in the table above, it can be analyzed that in comparison to the other enhancement algorithms and the EnlightenGAN+ algorithm, the mean PSNR, SSIM, and NIQE are increased by 12.3% and 0.7%, 57% and 10.3%, and 21% and 13%, respectively [27].

Our experiment shows that the original Enlighten GAN, LLNET, RetinexNet, and other algorithms can both improve the original image to different extents after the same training. The numerical results show that our improved algorithm performs well (slightly decreased in some places) under evaluation indices such as SSIM, PSNR, and NIQE. The difference in terms of the true visual effect of the image is that our algorithm has a better enhancement effect in some images with a complex distinction between light and dark. Our model can better improve the real areas that need improvement, but the enhancement effect of our model is not evident in some regions with a clear light–dark distinction.

5. Conclusions

This paper enhances laser images based on the idea of GAN. Firstly, it introduces the mainstream laser image enhancement techniques currently available. Subsequently, EnlightenGAN is introduced and three improvements are made to the original model. The first improvement establishes a connection between the global discriminator and local discriminator. The second involves an improved downsampling module. The third corrects the self-regularized attention mechanism under laser images. Then, ablation experiments and enhancement algorithm comparison experiments are designed. In the ablation experiment, our three improved modules have certain improvements under different evaluation indicators, especially after establishing the connection between the global discriminator and local discriminator, where the indicators all show significant improvement. When comparing the indicators of different algorithms, the EnlightenGAN+ algorithm that we propose shows an average improvement of 12.3% and 0.7% in PSNR and 57% and 10.3% in SSIM, and a decrease of 21% and 13% in NIQE. The experimental results show that our proposed model improves the signal-to-noise ratio and contrast of laser images, providing new ideas for the preprocessing of laser images and more detailed image information.

This paper introduces our achievements in the laser image enhancement algorithm so far. In view of some shortcomings of the current algorithm, we will continue to conduct related research on image processing using deep learning to achieve better image processing under more image conditions.

Author Contributions: Conceptualization, Y.F. and Y.W.; methodology, Y.F.; software, Y.W.; validation, K.F. and Y.L.; formal analysis, Y.F and H.W.; resources, Y.W.; data curation, Y.W.; writing—original draft preparation, Y.J.; writing—review and editing, J.X. and Y.N. and H.W.; supervision, J.X.; funding acquisition, Y.F. All authors have read and agreed to the published version of the manuscript.

Funding: This research was funded by Key Basic Research Projects of the Basic Strengthening Program, grant number 2020-JCJQ-ZD-071.

Data Availability Statement: Not applicable.

Conflicts of Interest: The authors declare no conflict of interest.

References

1. Wang, Y.; Liu, X. Low-resolution laser image enhancement method based on visual communication technology. *J. Lasers* **2022**, *43*, 121–125.
2. Lore, K.; Akintayo, A.; Sarkar, S. LLNet: A deep autoencoder approach to natural low-light image enhancement. *Pattern Recognit.* **2017**, *61*, 650–662. [CrossRef]
3. Li, C.; Guo, J.; Porikli, F.; Pang, Y. LightenNet: A Convolutional Neural Network for weakly illuminated image enhancement. *Pattern Recognit. Lett.* **2018**, *104*, 15–22. [CrossRef]
4. Chen, W.; Wang, W.; Yang, W.; Liu, J. Deep Retinex Decomposition for Low-Light Enhancement. In Proceedings of the British Machine Vision Conference, Newcastle, UK, 3 September 2018.
5. Liu, H.; Ye, H.; Xu, M.; Zhao, X. A review of generative adversarial network research. *Internet Things Technol.* **2022**, *12*, 93–97.
6. Zhu, J.; Park, T.; Isola, P.; Efros, A. Unpaired Image-to-Image Translation Using Cycle-Consistent Adversarial Networks. In Proceedings of the IEEE International Conference on Computer Vision (ICCV), Venice, Italy, 11–17 October 2017.
7. Ronneberger, O.; Fischer, P.; Brox, T. U-Net: Convolutional Networks for Biomedical Image Segmentation. In Proceedings of the Medical Image Computing and Computer-Assisted Intervention (MICCAI), Munich, Germany, 5–9 October 2015.
8. Yan, J.; Fang, Y.; Liu, X. A Review of Image Quality Evaluation Research—From the Perspective of Distortion. *J. Image Graph. China* **2022**, *27*, 1430–1466.
9. Yu, W. Research on blurred laser image enhancement based on visual communication technology. *J. Lasers* **2022**, *43*, 149–153.
10. Kou, X. Research on Group Game Technologies Based on Attention Mechanism and Entropy Regularization. Master's Thesis, Harbin Institute of Technology, Harbin, China, 2021.
11. Li, S. Research of Low-Light Image Enhancement Based on Enlightenment Generative Adversarial Network. Master's Thesis, Hunan University, Hunan, China, 2020.
12. Wang, M.; Zhang, H.; Li, J.; Zhang, C. Low-light image enhancement algorithm under mine based on deep neural network. *Coal Sci. Technol.* 1–13.
13. Lin, K.; Geng, J.; Cheng, W.; Li, A. Image dehazing algorithm based on attention mechanism and Markov discriminator. *Adv. Lasers Optoelectron.* **2022**, *59*, 112–119.

14. Nguyen, V.; Cai, J.; Wei, L.; Chu, J. Low-complexity probabilistic piecewise linear fitting of the Sigmoid function. *J. Xidian Univ.* **2020**, *47*, 58–65.
15. Jiang, Y.; Gong, X.; Liu, D.; Cheng, Y.; Fang, C.; Shen, X.; Yang, J.; Zhou, P.; Wang, Z. EnlightenGAN: Deep Light Enhancement Without Paired Supervision. *Trans. Img. Proc.* **2021**, *30*, 2340–2349. [CrossRef] [PubMed]
16. Zhang, Y.; Luo, S.; Chen, Y. Research on improved VGG vehicle type recognition based on attention mechanism. *Agric. Equip. Veh. Eng.* **2022**, *60*, 82–87.
17. Shen, Q. Research on Image Super-Resolution Algorithm Based on Generative Adversarial Networks. Master's Thesis, Nanjing University of Posts and Telecommunications, Nanjing, China, 2022.
18. Liu, J.; Tian, Y.; Fan, J. An image threshold segmentation method based on accumulated residual information energy. *Adv. Lasers Optoelectron.* **2023**, 1–19.
19. Bi, Y.; Xu, X. Research on underwater turbulence detection method based on laser distance gating technology. *J. Chang. Univ. Sci. Technol. Nat. Sci. Ed.* **2018**, *41*, 1–4.
20. Shao, X.; Zeng, T.; Wang, Z. A NIQE-based method for quality evaluation of printed images without reference. *J. Packag.* **2016**, *8*, 35–39.
21. Zhu, X.; Yao, S.; Sun, B.; Qian, Y. Image quality evaluation: Fusion of visual characteristics and structural similarity indicators. *J. Harbin Inst. Technol.* **2018**, *50*, 121–128.
22. Xiao, X.; Jing, W.; Zhao, H. Improved image enhancement algorithm based on peak signal-to-noise ratio. *J. Chang. Univ. Sci. Technol. Nat. Sci. Ed.* **2017**, *40*, 83–86+92.
23. Zhang, Y. Image Quality Assessment Based on Human Visual Perception. Ph.D. Thesis, Xidian University, Xi'an, China, June 2017.
24. Bao, K.; Meng, X.; Shao, F.; Ye, M.; Jin, K.; Peng, Z. MVG without reference quality evaluation of panchromatic/multispectral fusion images. *J. Remote Sens.* **2022**, *26*, 568–578.
25. Zhao, Y. Research on End-to-End Registration Method of UAV Aerial Images Based on Deep Learning. Ph.D. Thesis, North University of China, Shanxi, China, June 2022.
26. Khorasani, M.; Gibson, I.; Ghasemi, A.H. Laser subtractive and laser powder bed fusion of metals: Review of process and production features. *Rapid Prototyp. J.* **2023**, *29*, 935–958. [CrossRef]
27. Khorasani, M.; Ghasemi, A.; Leary, M. The effect of absorption ratio on meltpool features in laser-based powder bed fusion of IN718. *Opt. Laser Technol.* **2022**, *153*, 108263. [CrossRef]